HHS Public Access

Author manuscript

Sci Signal. Author manuscript; available in PMC 2018 March 15.

Published in final edited form as:

Sci Signal. ; 10(469): . doi:10.1126/scisignal.aah3737.

Cytoskeletal adaptivity regulates T cell receptor signaling

Timothy J. Thauland[1,2,*], **Kenneth H. Hu**[3], **Marc A. Bruce**[1], and **Manish J. Butte**[1,2,3,*,†]

[1]Stanford Immunology, Stanford University, Stanford, CA 94305, USA

[2]Division of Immunology, Allergy, and Rheumatology, Department of Pediatrics, Stanford University, Stanford, CA 94305, USA

[3]Stanford Biophysics, Stanford University, Stanford, CA 94305, USA

Abstract

The factors that govern T cell activation control the initiation and progression of adaptive immune responses. T cells recognize their cognate antigen on the surface of antigen-presenting cells (APCs) through the T cell receptor, which results in the formation of a contact region (immune synapse) between the two cells and the activation of the T cells. Activated T cells proliferate and differentiate into effector T cells that secrete cytokines, provide help to B cells, and kill target cells. We asked whether the actin cytoskeleton governs differences in signaling in effector T cells versus naïve (unstimulated) T cells. Using atomic force microscopy and quantitative confocal microscopy, we found that naïve T cells had a mechanically stiffer cortical cytoskeleton than that of effector cells, which resulted in naïve cells forming smaller immune synapses with APCs. This suggests that the cytoskeletal stiffness of the T cell before it undergoes antigen stimulation predicts its subsequent dynamic engagement with APCs and its activation potential. Cytoskeletal rigidity depended on the activity of the actin-severing enzyme cofilin through a pathway requiring the small guanosine triphosphatase RhoA and the kinases ROCK (Rho-activated kinase) and LIMK. These findings suggest that the baseline cytoskeletal state controls T cell responses and that the underlying pathway could be a therapeutic target for modulating adaptive immunity.

INTRODUCTION

T cells must maintain a threshold of activation that is low enough for them to rapidly scrutinize the body for sparse and low-affinity antigens, yet high enough to avoid triggering autoimmune responses. The cellular machinery that controls T cell activation also enables memory and effector T cells to be activated more readily than antigenically naïve cells, facilitating rapid effector responses upon reactivation (1–3). Here, we demonstrate that cytoskeletal differences in naïve and effector T cells affect their activation, and we define the molecular mechanisms underlying these differences.

[†]Corresponding author. mbutte@mednet.ucla.edu.

[*]Present address: Division of Immunology, Allergy, and Rheumatology, Department of Pediatrics, University of California, Los Angeles, Los Angeles, CA 90095, USA.

Author contributions: T.J.T. and M.J.B. conceptualized the study; M.A.B. developed the required software; T.J.T., K.H.H., M.A.B., and M.J.B. performed experiments; T.J.T. and M.J.B. performed imaging studies; T.J.T. and M.J.B. wrote the manuscript; and M.J.B. supervised the study.

Competing interests: The authors declare that they have no competing interests.

When T cell receptors (TCRs) recognize their cognate antigens on the surface of an antigen-presenting cell (APC), a series of cytoskeleton-dependent events are stimulated in the T cells that are critical for full activation. At the cellular scale, T cells stop crawling, turn to reorient their microtubule-organizing center toward the interface between the T cell and the APC, expand lamellipodia over (4), and forcefully push into APCs (5–7), increasing the surface area of the cell-cell contact and enhancing TCR signaling. The nanoscale changes at the T cell–APC interface result in the assembly of an immune synapse (8), starting with the gathering of TCRs into microclusters, the formation of which depends on actin polymerization (9). Thus, the actin cytoskeleton is important for forming and maintaining the cell-cell interface, as well as for gathering the key signaling molecules required for T cell activation. Whether differences in cytoskeletal regulation between naïve and effector cells mediate their differential activation has not been investigated; however, activated T cells and memory cells have preformed nanoclusters of TCRs on the cell membrane (10). These nanoclusters, which do not occur in naïve cells, facilitate signaling and are organized by cytoskeletal molecules (11). Furthermore, effector and memory T cells have increased amounts of transcripts encoding cytoskeletal molecules, including actin, talin, Arp2/3, and stathmin (12, 13).

Here, we examined the cytoskeletal pathway downstream of the Rho family member RhoA (14). The active, guanosine triphosphate (GTP)–bound form of RhoA binds to and activates members of the Rho kinase (ROCK) family of serine and threonine kinases (15). ROCK mediates T cell crawling and polarization (16) and phosphorylates multiple downstream cytoskeletal regulators, including LIM kinase (LIMK) (17). LIMK, in turn, inhibits cofilin, an actin-severing and actin-depolymerizing enzyme. Upon TCR stimulation, cofilin is activated by phosphatases, which enhances actin branching and actin polymerization and is necessary for immune synapse formation (18).

Here, we tested the hypothesis that cytoskeletal pathways modulate immune synapse size and thus regulate T cell activation. Using atomic force microscopy (AFM) and confocal microscopy to assess the single-cell responses of T cells to stimulation, we found that naïve mouse $CD4^+$ T cells, at baseline, had increased cytomechanical stiffness compared to that of effector $CD4^+$ T cells because of increased activity of the RhoA-ROCK-LIMK-cofilin axis. Modulation of molecules in this axis led to the enhanced activation of naïve T cells and decreased effector T cell activation with corresponding changes in cytomechanical stiffness. Our results suggest that this cytoskeletal pathway governs the ability of T cells to intimately engage APCs, and thus modulates T cell activation. These findings also suggest re-envisioning the cytoskeleton as an active, mechanical rheostat of cellular signals.

RESULTS

Effector $CD4^+$ T cells form larger immune synapses than those formed by naïve cells

There is compelling evidence that effector $CD4^+$ T cells are more responsive to antigen than naïve T cells (1). To determine whether early signaling events are also enhanced in effector T cells, we measured Ca^{2+} flux in naïve and effector OT-II T cells that interacted with antigen-loaded APCs. OT-II T cells are from TCR transgenic mice and recognize a peptide from ovalbumin in the context of the I-A^b major histocompatibility complex molecule. We

found that effector T cells fluxed substantially more Ca^{2+} than did naïve T cells (Fig. 1A and fig. S1, A to C). We hypothesized that the enhanced activation of effector cells correlated with improved contact between the T cells and APCs. To test this idea, we examined the immune synapses formed by naïve and effector T cells. We identified functional T cell–APC conjugates through the accumulation of protein kinase C-θ (PKC-θ) at the immune synapse. The accumulation of the integrin leukocyte function–associated antigen 1 (LFA-1) was used to determine the extent of the T cell–APC interface, as measured by the volume of positive pixels. Of course, effector T cells are larger than naïve cells, and so it would be expected that their absolute contact area with APCs would be larger. To address this concern, we measured the LFA-1^+ pixel volumes of naïve and effector cells that were not engaged with APCs and used these measurements to scale the sizes of the immune synapse. After normalization, we still found that a larger fraction of the total surface area was at the immune synapse in effector cells (Fig. 1, B and C).

To determine whether the antigen-stimulated changes in immune synapse size correlated with cytoskeletal stiffness, we directly measured the elastic moduli of T cells by AFM. At indentation depths of a few hundred nanometers, the elastic modulus correlates with the local actin density and the degree of tethering of cortical actin to the plasma membrane (19). Furthermore, in these measurements, the rigidity of the plasma membrane is negligible compared to that of the cytoskeleton (20). We started by assessing the elastic moduli of live T cells (fig. S2A). Fitting these measurements of local indentation (fig. S2B) revealed that the mean elastic modulus of naïve T cells was about fourfold higher than that of effector T cells (Fig. 1D). Thus, naïve T cells are stiffer than effector T cells. To study whether these differences in stiffness were local or global, we evaluated stiffness across whole T cells by force-distance nanoindentation mapping. Naïve or effector T cells were gently fixed, and hundreds of force-distance touches across each T cell were performed with an uncoated AFM cantilever (fig. S2C). Naïve T cells were much stiffer, with an about sixfold higher median elastic modulus than that of effector cells (Fig. 1E), which was consistent with the live-cell measurements.

We attempted to account for the differences in stiffness that we observed by comparing F-actin content in naïve and effector T cells, which we analyzed by flow cytometry and normalized for cell size. We found that effector cells contained 1.3-fold more F-actin than did naïve cells (fig. S3A). Colocalization analyses showed that the amount of F-actin associated with LFA-1^+ voxels at the immune synapse was greater in effector T cells than in naïve T cells (fig. S3B). The larger synapses formed by effector cells and the increase in F-actin abundance in the immune synapses formed by these cells suggest that actin regulation is more dynamic in effector cells than in naïve T cells. Therefore, we endeavored to measure pathways known to modulate the actin cytoskeleton in T cells.

ROCK is more active in naïve T cells than in effector T cells

Our AFM measurements probed the cytoskeletal structure underneath the plasma membrane. Therefore, we examined cytoskeletal pathways that might account for the localized differences in cytoskeletal stiffness between naïve and effector cells. We decided to measure ROCK abundance and activity, because a number of cytoskeletal molecules are regulated by

ROCK (15). At the transcriptional level, others have found that *ROCK1* mRNA amounts are similar between naïve T cells and T helper 1 (T_H1) effector cells [Gene Expression Omnibus: GSE32901 (21)]. Similarly, we found that the amounts of ROCK protein were comparable in naïve and effector T cells (Fig. 2A). However, an in vitro kinase assay revealed that the activity of ROCK isolated from naïve T cells was ~2.5-fold higher than that of ROCK isolated from effector T cells (Fig. 2B).

To understand this difference in ROCK activity, we examined the activity and localization of the Rho family member RhoA in naïve and effector T cells. We found that active (GTP-bound) RhoA was threefold more abundant in naïve cells than in effector cells (Fig. 2C). The activation of RhoA leads to its translocation from the cytosol to the plasma membrane (22). Furthermore, RhoA activity directly proximal to the plasma membrane corresponds to the region that we analyzed in our AFM experiments. We examined the colocalization of RhoA with cortical F-actin as a surrogate for its plasma membrane proximity. We found that more RhoA was localized at the plasma membrane in naïve T cells than in effector T cells (Fig. 2D), and that there was substantially greater overlap between cortical actin and RhoA in naïve cells than in effector T cells (Fig. 2E). These results suggest that the increased activity of ROCK in naïve cells is caused by the differential organization and increased activity of RhoA in naïve cells compared to that in effector T cells.

Inhibiting ROCK or LIMK in naïve T cells promotes T cell activation

We hypothesized that the inhibition of ROCK or LIMK and the resulting increase in cofilin activity would reduce the stiffness of naïve T cells, enhance the size of the immune synapses that they formed, and increase their activation (Fig. 3A). Inhibiting ROCK in naïve T cells with glycyl-H-1152 resulted in a >90% reduction in the abundance of phosphorylated cofilin (fig. S4A). Naïve T cells treated with the ROCK inhibitor formed larger immune synapses than those formed by untreated control cells (Fig. 3B and fig. S4B), and they had a decreased elastic modulus, as shown by experiments with fixed (Fig. 3C) and live cells (fig. S4C). To determine whether the formation of larger immune synapses was functionally important, we measured Ca^{2+} flux in response to antigenic stimulation. Naïve T cells treated with the ROCK inhibitor showed an increased Ca^{2+} flux compared to that of control cells (Fig. 3D and fig. S5). ROCK has many targets that could plausibly influence the cytoskeleton (15); however, we decided to investigate LIMK, because it is the principal kinase responsible for the inactivation of cofilin (17). Naïve T cells treated with a LIMK inhibitor (LIMKi 3) had greatly reduced cofilin phosphorylation (fig. S6A), decreased elastic moduli (fig. S4C), and increased Ca^{2+} flux (Fig. 3E and fig. S6B) compared to control cells. Furthermore, Western blotting analysis of naïve T cells stimulated by peptide-loaded APCs revealed that the tyrosine phosphorylation of proteins in cells treated with the LIMK inhibitor was greater in extent than that of control cells (Fig. 3F and fig. S6C). These results suggest that LIMK is the relevant target of ROCK inhibition and support the idea that LIMK acts as a brake on cofilin-dependent immune synapse formation and T cell activation.

Cofilin is rapidly dephosphorylated upon TCR stimulation and controls T cell stiffness, immune synapse size, and T cell activation

Cross-linking the TCR and the costimulatory receptor CD28 on human peripheral blood T cells for 30 to 60 min reduces the phosphorylation of the inhibitory Ser^3 residue on cofilin (23). To determine whether cofilin was activated at much earlier times, we evaluated Ser^3 dephosphorylation in the first few minutes after stimulation. We found that both naïve and effector T cells rapidly dephosphorylated cofilin within 1 to 5 min when strong signals were delivered through the TCR and CD28 (Fig. 4A). To determine whether TCR stimulation altered the biomechanical properties of the cells, we measured naïve T cells by AFM after they were cultured on a stimulatory surface for 1 hour and found that activated T cells were substantially softer than control cells interacting with a non-stimulatory surface (Fig. 4B). Further experiments demonstrated that marked T cell softening occurred between 10 and 30 min after activation (fig. S7). In vivo, T cells make multiple, relatively short-lived contacts with APCs during the first hours of an immune response (24). We hypothesized that strong signals during the initial interactions between T cells and APCs are sufficient to activate cofilin and induce cytomechanical softening, leading to enhanced signaling during subsequent contacts in a positive feedback loop.

To examine the role of cofilin in maintaining a pliable cytoskeleton in effector T cells, we transduced the cells with retrovirus expressing short hairpin RNA (shRNA) to knock down cofilin (fig. S8A). We hypothesized that knocking down cofilin in effector T cells would increase cellular stiffness, decrease immune synapse size, and reduce cellular activation (Fig. 4C). Effector T cells expressing cofilin-specific shRNA were mechanically stiffer (Fig. 4D) and formed smaller immune synapses when compared to cells expressing control shRNA (fig. S8B). Furthermore, knocking down cofilin rendered the effector T cells refractory to activation by peptide-loaded APCs (Fig. 4E). To assess whether the phosphorylation of cofilin directly inhibited T cell activation, we transduced T cells with a control retrovirus, a retrovirus expressing wild-type (WT) cofilin, or a retrovirus expressing a phosphomimetic mutant cofilin (S3D), following an approach previously used in experiments with B cells (25). We found a substantial decrease in TCR-stimulated tyrosine phosphorylation in cells bearing the S3D mutant cofilin compared to that in cells expressing WT cofilin (fig. S8C). Together, these results suggest that cofilin activity maintains the mechanics and activity of effector T cells.

Increasing ROCK activity in effector T cells dampens their activation

Finally, we assessed whether the relatively reduced ROCK activity in effector T cells was responsible for their enhanced activation by evaluating the effect of increasing ROCK activity in these cells. We hypothesized that increasing ROCK activity in effector T cells would stiffen the cells, resulting in reduced immune synapse size and decreased activation (Fig. 5A). We transduced effector $CD4^+$ T cells with retroviruses expressing either WT ROCK2 or a constitutively active mutant ROCK2 (ROCK CAT) (Fig. 5B) and performed AFM measurements that showed that the ROCK CAT–expressing T cells were twice as stiff as the cells that expressed WT ROCK2 (Fig. 5C) and formed substantially smaller immune synapses (Fig. 5D and fig. S9). Finally, we assessed whether the reduction in immune synapse size in these cells affected T cell activation, and we found that the ROCK CAT–

expressing cells exhibited substantially reduced Ca^{2+} flux compared to that in cells expressing WT ROCK2 (Fig. 5E). Together, these results suggest that enhancing the activity of ROCK in effector T cells increased their stiffness, reduced immune synapse size, and dampened cellular activation.

DISCUSSION

Here, we applied AFM to correlate cytoskeletal stiffness with immune synapse formation and TCR stimulation. Our studies suggest that signaling through the RhoA-ROCK-LIMK-cofilin pathway increases cytoskeletal rigidity, which substantially influences the size of the immune synapse in T cells engaged with APCs. We found that the baseline cytoskeletal stiffness correlated with the eventual size of the immune synapse and the strength of signaling proximal to the TCR, and we propose a model for the relationship between stiffness and T cell activation (fig. S10).

The dephosphorylation of cofilin in T cells requires costimulatory signals through CD28 (26), and there may be two routes further downstream that lead to cofilin activation. First, a Ras–phosphoinositide 3-kinase (PI3K) pathway mediates cofilin dephosphorylation (27). Second, the Rap family of guanosine triphosphatases (GTPases) is implicated in cofilin regulation, because cofilin dephosphorylation, which is required for the spreading of A20 cells and Jurkat cells on stimulatory surfaces, is inhibited by overexpression of a dominant-negative Rap (25). Effector cells are less dependent on costimulation than naïve cells (1). Our data may provide an explanation for this phenomenon: Activated cells are already relatively soft in the steady state and thus able to form large, intimate contacts with APCs without PI3K-mediated activation of cofilin downstream of costimulatory receptors. On the other hand, the rigidity of naïve cells may act as a check on activation by conferring a dependence on costimulation. This biomechanical brake may serve to prevent inappropriate responses to antigen in the absence of optimal costimulation. For example, in some experimental systems with TCR-encoding transgenes, naïve T cells are not easily activated by self-antigens (28, 29).

Our results, and those from a previous study (30), suggest that there are multiple mechanisms that control the rigidity of T cells. Faure *et al.* showed that transfection of T cells with plasmid encoding a constitutively active RhoA causes increased phosphorylation of members of the ezrin, radixin, and moesin (ERM) family of proteins and cell rigidity, as measured by deformation on a glass coverslip (30). Whereas this result was interpreted as evidence that RhoA increases cellular rigidity through the phosphorylation of ERM proteins, we consider it likely that the RhoA-mediated activation of ROCK contributes to the effect. The earlier study did not address the role of ERM proteins in naïve cells, because the experiments were performed in transduced, activated T cells, whereas the experiments in our study highlight the importance of cellular rigidity in naïve T cells. Because both ERM-dependent and ROCK-dependent pathways may control immune synapse formation, further experiments will be necessary to discern their relative importance.

We showed that RhoA was more active and membrane-proximal in naïve T cells than in activated T cells, but the factors governing this differential RhoA activity are unknown.

RhoA activity is enhanced by guanine nucleotide exchange factors and inhibited by GTPase activating proteins and Rho guanine nucleotide dissociation inhibitors. There are at least 30 such RhoA regulators in T cells (31). The signaling pathways responsible for the differential regulation of cofilin in naïve and effector cells are also not yet fully understood but may be related to differences in the activities of the phosphatase that activates cofilin. Although our work indicates that LIMK and cofilin are key effector molecules downstream of ROCK, other ROCK targets could also be important for regulating the stiffness of T cells, including adducin, which tethers actin to the plasma membrane and is phosphorylated upon TCR stimulation (32). Coronin also plays an important role in F-actin turnover in T cells, although whether it has differential activity after activation is not yet known (33). Similarly, gelsolin is an actin-severing enzyme that is increased in activity upon TCR stimulation (34). As we showed here, AFM could be used to study the effects of these molecules on cytoskeletal rigidity.

Differential regulation of ROCK and cofilin may alter the organization and dynamics of the TCR. Cofilin activity is required for the enhanced mobility of single B cell receptors (BCRs) and BCR microclusters upon treatment with lipopolysaccharide (25, 35). A similar phenomenon may exist in activated T cells. Freeman *et al.* also noted that ex vivo marginal zone B cells have a lower threshold for activation after exposure to antigen and exhibit reduced cofilin phosphorylation when compared to follicular B cells (35). AFM experiments could be conducted to determine whether marginal zone B cells are cytomechanically softer than follicular B cells, which would reveal whether our findings concerning the relationship between mechanical properties and activation are generalizable across all lymphocytes.

In conclusion, this work suggests that cytoskeletal stiffness controls T cell activation by modulating the intimate contacts formed with APCs. The cytoskeletal pathway identified here, which is responsible for modulating stiffness and T cell reactivity, should be considered a potential therapeutic target for controlling T cell–mediated diseases. Whereas modulation of ROCK activity is complicated by the multitude of available ROCK substrates, which control a range of cellular processes, the only known substrates of LIMK are members of the cofilin family of proteins, making LIMK an ideal target for therapeutic intervention.

MATERIALS AND METHODS

Mice, cell lines, and reagents

WT mice (C57BL/6NTac) and OT-II TCR transgenic mice were purchased from Taconic Biosciences. The I-A^{b+} B cell lymphoma line LB27.4 was purchased from the American Type Culture Collection. The following antibodies were used in this study: anti–PKC-θ (C-18), anti-ROCK (H-85), anti-RhoA (clone 26C4), and anti–β-actin–HRP (horseradish peroxidase) (clone C4) were from Santa Cruz Biotechnology; anti–phospho-cofilin (Ser^3, clone 77G2), anti-cofilin (clone D3F9), anti–Zap-70 (clone D1C10E), and anti–SLP-76 (#4958) were from Cell Signaling Technology; anti-human CD25 (clone BC96) and anti-CD28 (clone 37.51) were from BioLegend; anti–LFA-1 (clone I21/7) was from Southern Biotechnology; anti-phosphotyrosine (4G10) was from EMD Millipore; anti-CD3ε (clone 145-2C11) was from BioXCell; and Alexa Fluor 568 phalloidin was from Life Technologies.

Ovalbumin peptide 323–339 was obtained from AnaSpec. Recombinant murine interleukin-7 (IL-7) was obtained from PeproTech, whereas recombinant human IL-2 was from Prometheus. Here, we used glycyl-H-1152, a highly specific, small-molecule ROCK inhibitor (Tocris) at a final concentration of 100 nM. In contrast, other studies of ROCK inhibition have used the low-potency inhibitor Y-27632, which requires high micromolar concentrations to see any effect in cells and is subject to off-target effects on other intracellular kinases important for T cells, including the PKC-associated kinase PRK2 (36). The LIMK inhibitor LIMKi 3 was also obtained from Tocris and was used at a final concentration of 1 μM. Cells were incubated with inhibitors for 1 hour at 37°C and then were washed before being used in assays to remove excess inhibitor.

T cell activation and retroviral transduction

$CD4^+$ T cells were purified from spleens and lymph nodes by EasySep immunomagnetic negative selection (STEMCELL Technologies). Cells were activated on plates coated with anti-CD3ε antibody (10 μg/ml) in the medium supplemented with anti-CD28 antibody (2 μg/ml) and recombinant murine IL-7 (2 ng/ml). Effector T cells were removed from wells coated with anti-CD3ε, allowed to proliferate in IL-2–containing medium, and then used for experiments on days 3 to 5 of incubation. For retroviral transduction, T cells were spinfected about 24 and 36 hours later. After the second spinfection, the cells were moved to new wells lacking anti-CD3ε and were rested overnight. Platinum E cells were transfected with murine stem cell virus (MSCV) retroviral vectors expressing WT cofilin, a mutant cofilin in which Ser^3 was replaced with aspartic acid (S3D), or a truncated form of murine ROCK2 corresponding to amino acids 2 to 727 (37). These vectors also contained the nonsignaling extracellular domain of human CD25 under the control of the *Pgk1* promoter. MSCV vectors expressing only hCD25 were used as controls. One day after transfection, the medium was removed from the Platinum E cells and replaced with T cell medium. Two days after transfection, virus-containing cell culture medium was removed and concentrated about 10-fold (Amicon Ultra-15; 100,000 molecular weight cutoff). Concentrated viral samples were added directly to wells of T cells in the presence of polybrene (8.0 μg/ml) and spinfected at 800*g* for 90 min at 37°C. Supernatants were removed, and T cell medium containing IL-2 (50 U/ml) was added back to the wells. For the cofilin knockdown experiments, Platinum E cells were transfected with an LMP retroviral vector expressing green fluorescent protein (GFP) and a miR-30–based shRNA targeting the following sequence in the 3′ untranslated region of *Cfl1*: GGTTCTGTGTGTAAATGAA. T cells were spinfected, as described earlier, except that virus-containing cell culture medium was not concentrated. As a control, the $CD4^+$ T cells were transduced with vectors expressing an shRNA targeting CD8, as described previously (38). GFP^+ cells were sorted, and the extent of knockdown of cofilin 1 was confirmed by Western blotting analysis.

Western blotting analysis

Cells were lysed in radioimmunoprecipitation assay buffer containing Halt Protease inhibitor cocktail (Life Technologies) and PhosphataseArrest I (G-Biosciences). After centrifugation, the soluble fractions of lysates were resolved by SDS–polyacrylamide gel electrophoresis and proteins were transferred to polyvinylidene difluoride membranes. Membranes were blocked with phosphate-buffered saline (PBS)–Tween 20 containing 5% bovine serum

albumin and incubated with the appropriate primary and HRP-conjugated secondary antibodies (GE Healthcare). SuperSignal West Pico (Life Technologies) and Western Lightning ECL Pro (PerkinElmer) were used as chemiluminescent substrates. In some experiments, T cells were added to 96-well plates coated with anti-CD3ε (10 μg/ml) and anti-CD28 (5 μg/ml), centrifuged for 1 min at 100*g*, and incubated at 37°C for the times indicated in the figure legends. To stop the stimulation, we added SDS loading buffer containing sample reducing agent directly to the wells (Life Technologies). In stimulation experiments with APCs, LB27.4 B cells were loaded with 1 μM ovalbumin peptide for 1 hour at 37°C. The T cells and the LB27.4 cells were serum-starved for 15 min at 37°C and subsequently kept on ice in serum-free RPMI. To initiate conjugation, we combined the T cells and the LB27.4 cells at a 1:1 ratio and centrifuged at 4°C for 1 min at 500*g*. The cells were then placed in a 37°C water bath for 5 min. After cell-cell conjugation had occurred, the cells were lysed by the addition of SDS loading buffer containing sample reducing agent directly to the tubes.

ROCK and RhoA activity assays

Cleared cell lysates from naïve and effector T cells were incubated overnight with 1 μg of anti-ROCK antibody at 4°C. Antibody-antigen complexes were coupled to protein A/G agarose with the Pierce Classic IP kit (Life Technologies). We used a ROCK activity immunoblot kit (Cell Biolabs) to assay the activity of ROCK pulled down from naïve and effector lysates, according to the manufacturer's instructions. After phospho-MYPT1 (a ROCK target) was detected by Western blotting, the blots were stripped and incubated with an antibody against β-actin, which was used as a loading control. The colorimetric RhoA G-LISA Activation Assay Kit (Cytoskeleton Inc.) was used to measure the amount of GTP-bound RhoA in the lysates of naïve and effector T cells. Lysates were prepared, and protein concentrations were measured with the provided reagents. Protein concentration was normalized (0.4 mg/ml) for all samples, and each sample was analyzed in duplicate, as per the manufacturer's instructions. The protein concentration of the normalized samples was confirmed with the Pierce BCA Protein Assay Kit (Thermo Scientific).

Microscopic analysis of immune synapses and protein colocalization

Naïve or effector $CD4^+$ T cells were combined with LB27.4 B cells that had been loaded with 1 μM ovalbumin, centrifuged for 1 min at 500 *g*, and incubated at 37°C for 5 min. Cell pellets were gently disrupted and centrifuged for 1 min at 50*g* onto Lab-Tek II eight-well chamber slides coated with poly-D-lysine. After fixation with 4% paraformaldehyde (PFA), cell-cell conjugates were permeabilized with 0.1% Triton X-100 and blocked overnight in PBS containing 5% donkey serum. The wells were stained with antibodies against PKC-θ and LFA-1 and with Alexa Fluor 568–conjugated phalloidin. In some experiments, the wells were incubated with antibodies against hCD25 to identify transduced cells. After washing, the wells were incubated with fluorescently conjugated secondary antibodies (Jackson ImmunoResearch). The specimens were covered with Fluoromount-G (eBioscience) and stored at 4°C until imaging was performed. Conjugates were selected for imaging based on PKC-θ accumulation at the T cell–APC interface. Conjugates were imaged with a 100× Plan Apo numerical aperture (NA) 1.4 objective (Nikon) on a system that includes a Nikon Ti-E chassis; a Yokugawa CSU-X1 spinning disc confocal; 405-, 488-, 561-, and 641-nm lasers; a

motorized *z*-axis piezoelectric stage (Applied Scientific); and an XR/MEGA-10EX camera (Stanford Photonics). The system was controlled by Micro-Manager software. We captured 0.2-μm axial slices through the conjugates. Individual T cell–APC conjugates were cropped in Fiji software and run through a homemade Macro in Fiji that thresholded the LFA-1 image. For colocalization analysis, naïve and effector (day 3) T cell conjugates were fixed with 4% PFA, permeabilized with 0.1% Triton X-100, and blocked overnight in PBS containing 5% donkey serum. The cells were stained with Alexa Fluor 488–conjugated anti-RhoA and Alexa Fluor 568–conjugated phalloidin. The specimens were covered with Fluoromount-G and stored in the dark at 4°C until required for imaging. Z-stacks were captured with 0.2-μm axial slices as described earlier. Images were subjected to GPU deconvolution (39) with a calculated point spread function (Microvolution) and background-subtracted in Fiji. For colocalization measurements, we used the Confined Displacement Algorithm implemented in the GDSC Stack Colocalization plugin in Fiji to calculate the Manders coefficient for regions of the images that were selected by the MaxEntropy thresholding method with default parameters (100 permutations; minimum shift, 9; maximum shift, 16; significance, 0.05). To calculate the Pearson correlation coefficient between actin and LFA-1 enriched in the immune synapse, we used the GDSC Stack Correlation plugin.

Ca^{2+} flux measurements

T cells were loaded with Fluo-4 (1.0 μM) and Calcein Red-Orange (0.2 μM) as per the manufacturer's protocol (Life Technologies). Calcein is insensitive to calcium in the physiological range for T cells, and this helped in the location of T cells in Imaris software. Labeled T cells and LB27.4 cells loaded with ovalbumin peptide were introduced to Delta T dishes that kept the media warmed to 37°C. To reduce cell drift, we used imaging media containing 0.3% low melting point agarose. Fields were imaged every 12 or 15 s for about 20 min with a 40× Plan Fluor NA 0.6 extra long working distance objective objective (Nikon). We used wide-field microscopy on a similar setup to that used for immune synapse analysis, except that we used a Sutter Lambda XL lamp and the appropriate filter sets (Chroma Technology). Imaris software (Bitplane) was used to track Calcein Red-Orange–loaded T cells and to assess Fluo-4 fluorescence over time. Fold changes in Fluo-4 fluorescence were calculated by dividing the maximum fluorescence by the fluorescence at time 0. Ca^{2+} fluxes were excluded if the increase was less than 1.25-fold, the increase in Ca^{2+} concentration lasted less than 1 min, or the Ca^{2+} flux was from a T cell that was observed for less than 5 min. In a pseudoratiometric fashion, we examined the Calcein Red-Orange signal throughout the experiments, and we saw no statistically significant changes, which removed concerns that changes in the cell shape, volume, or focal plane influenced our interpretation of Ca^{2+} flux. Only transduced cells that engaged an APC were included in the analysis. For experiments with cells transduced with control virus or virus expressing ROCK2 CAT, the cells were labeled with phycoerythrin (PE)–conjugated anti-human CD25 antibody on ice and washed after the cells were loaded with Fluo-4. Cells were dropped into heated Delta T dishes coated with anti-CD3ε (500 ng/ml) and imaged as described earlier. Only cells that had a clear PE signal, that is, those that had been transduced, were included in the analysis.

AFM measurements

AFM experiments were performed on an MFP-3D-BIO atomic force microscope (Asylum Research) attached to a Nikon Ti-E fluorescence microscope. We used SHOCON and SHOCON-G cantilever tips (Applied NanoStructures) for stiffness measurements. For elastic moduli measurements, cells were plated onto glass-bottom petri dishes (FluoroDish) coated with poly-D-lysine and fixed with PBS containing 2% PFA for 15 min at room temperature. For the activation experiments shown in Fig. 4B, naïve $CD4^+$ T cells were added to FluoroDishes coated with anti-CD3ε (10 μg/ml) and poly-D-lysine and were incubated for 1 hour at 37°C, washed with PBS, and fixed with PBS containing 2% PFA for 15 min at room temperature. For the live-cell experiments shown in Fig. 1D, both naïve and day 4 effector T cells were placed into medium in warmed (37°C), poly-D-lysine–coated FluoroDishes. Force curves were generated by indenting cells with a SHOCON cantilever to a trigger point of 200 pN. We averaged five measurements per live-cell measurement. Elastic moduli maps were measured using the Force Map mode of the Asylum control software. To make these maps, we used contact-mode AFM nanoindentation to measure an average of 200 points on each cell. Settings were all at default values, except that we used an approach velocity of 750 nm/s, a trigger point of 100 to 150 pN, and a return height of 2 to 3 μm. T cells were ~5 μm high and indented to a depth of 100 to 400 nm, creating a local strain on the cell of less than 10% to minimize the effect of substrate-related artifacts. To determine the elastic modulus at each point of the force map, we used a Hertzian analysis to relate force to indentation. Taking the geometry of the SHOCONG cantilevers into account, the Hertzian-type equation for an ideal pyramidal indenter (40) was used. The point along the extension at which contact was made with the cells could not be known ab initio, so we included the point of contact as a fitted parameter in addition to the elastic modulus. For the silicon-tipped cantilevers used, the elastic modulus of the tip was 150 GPa, the Poisson value was 0.17, and the cone half-angle was 20°. The Poisson value for the cell was assumed to be 0.5 (incompressible). To measure the reproducibility of the scans and to ensure that the tip geometry was not altered, we scanned the cells continuously for 4 days and then analyzed the tip by scanning electronic microscopy. Repeatedly scanning the same cell gave highly reproducible results (fig. S11A), and we found that the tip geometries (radius of curvature and shape) were unchanged after 4 days of continuous scanning (fig. S11B). To calculate elastic moduli, we wrote a custom program that used the Ceres Solver library (41) to perform nonlinear least squares curve fitting. To extract only the portions of the force map corresponding to the cells and not the substrate (glass), we first flattened the height maps with Asylum software such that the height of the glass was, on average, 0 μm. Next, we masked the cell by removing all points of contact at which the height registered below 50 nm or where there was less than 5 nm of indentation. The data were then exported to R for analysis and plotted with the ggplot package. The distributions of stiffness measurements for each cell were clearly not normal or log-normal, although we displayed them on a $\log_{10}$ scale for visual clarity.

Statistical analysis

Permutation testing was used for all statistical comparisons of Ca^{2+} flux, immune synapse size, fluorescence colocalization, and cellular stiffness. This method reduced the potential influence of outliers and relaxed the requirement of knowing the distribution of observations

by comparing the value of the test statistic to a reference distribution generated from the data themselves, rather than to a standard distribution. To ensure that permutation testing was a suitable way to compare means, we showed first that the variances of the two groups were similar by the nonparametric Ansari-Bradley test with a *P* value cutoff of 0.05 (in the "stats" package of R). We used the permutationTest2 function of the "resample" package of R to calculate *P* values and determine the 95% CIs, performing 50 to 100,000 permutations. Boxes in all figures show the bootstrapped mean and 95% CI.

Supplementary Material

Refer to Web version on PubMed Central for supplementary material.

Acknowledgments

We thank D. B. Lewis, M. M. Davis, and P. L. Bollyky for critical feedback on the manuscript. Cell sorting for this project was performed on instruments in the Stanford Shared FACS Facility.

Funding: Financial support for this work came from the NIH/National Institute of Allergy and Infectious Diseases (K08 AI079268), NIH/National Institute of General Medical Sciences (R01 GM110482), the Stanford Child Health Research Institute, the Morgridge Family Foundation, and the NSF (CBET 1264833) (all to M.J.B.) and T32 GM008294 (to K.H.H.).

REFERENCES AND NOTES

1. Iezzi G, Karjalainen K, Lanzavecchia A. The duration of antigenic stimulation determines the fate of naive and effector T cells. Immunity. 1998; 8:89–95. [PubMed: 9462514]
2. Huang J, Brameshuber M, Zeng X, Xie J, Q-j Li, Chien Y-h, Valitutti S, Davis MM. A single peptide-major histocompatibility complex ligand triggers digital cytokine secretion in $CD4^+$ T cells. Immunity. 2013; 39:846–857. [PubMed: 24120362]
3. Rogers PR, Huston G, Swain SL. High antigen density and IL-2 are required for generation of CD4 effectors secreting Th1 rather than Th0 cytokines. J Immunol. 1998; 161:3844–3852. [PubMed: 9780149]
4. Negulescu PA, Krasieva TB, Khan A, Kerschbaum HH, Cahalan MD. Polarity of T cell shape, motility and sensitivity to antigen. Immunity. 1996; 4:421–430. [PubMed: 8630728]
5. Sage PT, Varghese LM, Martinelli R, Sciuto TE, Kamei M, Dvorak AM, Springer TA, Sharpe AH, Carman CV. Antigen recognition is facilitated by invadosome-like protrusions formed by memory/effector T cells. J Immunol. 2012; 188:3686–3699. [PubMed: 22442443]
6. Ueda H, Morphew MK, McIntosh JR, Davis MM. $CD4^+$ T-cell synapses involve multiple distinct stages. Proc Natl Acad Sci USA. 2011; 108:17099–17104. [PubMed: 21949383]
7. Hu KH, Butte MJ. T cell activation requires force generation. J Cell Biol. 2016; 213:535–542. [PubMed: 27241914]
8. Dustin ML. Hunter to gatherer and back: Immunological synapses and kinapses as variations on the theme of amoeboid locomotion. Annu Rev Cell Dev Biol. 2008; 24:577–596. [PubMed: 18598213]
9. Campi G, Varma R, Dustin ML. Actin and agonist MHC–peptide complex–dependent T cell receptor microclusters as scaffolds for signaling. J Exp Med. 2005; 202:1031–1036. [PubMed: 16216891]
10. Kumar R, Ferez M, Swamy M, Arechaga I, Rejas MT, Valpuesta JM, Schamel WWA, Alarcon B, van Santen HM. Increased sensitivity of antigen-experienced T cells through the enrichment of oligomeric T Cell receptor complexes. Immunity. 2011; 35:375–387. [PubMed: 21903423]
11. Klammt C, Lillemeier BF. How membrane structures control T cell signaling. Front Immunol. 2012; 3:291. [PubMed: 23055999]
12. Kaech SM, Hemby S, Kersh E, Ahmed R. Molecular and functional profiling of memory CD8 T cell differentiation. Cell. 2002; 111:837–851. [PubMed: 12526810]

13. Liu K, Li Y, Prabhu V, Young L, Becker KG, Munson PJ, Weng N-p. Augmentation in expression of activation-induced genes differentiates memory from naive $CD4^+$ T cells and is a molecular mechanism for enhanced cellular response of memory $CD4^+$ T cells. J Immunol. 2001; 166:7335–7344. [PubMed: 11390484]
14. Heasman SJ, Ridley AJ. Multiple roles for RhoA during T cell transendothelial migration. Small GTPases. 2010; 1:174–179. [PubMed: 21686273]
15. Amano M, Nakayama M, Kaibuchi K. Rho-kinase/ROCK: A key regulator of the cytoskeleton and cell polarity. Cytoskeleton. 2010; 67:545–554. [PubMed: 20803696]
16. Rougerie P, Delon J. Rho GTPases: Masters of T lymphocyte migration and activation. Immunol Lett. 2012; 142:1–13. [PubMed: 22207038]
17. Maekawa M, Ishizaki T, Boku S, Watanabe N, Fujita A, Iwamatsu A, Obinata T, Ohashi K, Mizuno K, Narumiya S. Signaling from Rho to the actin cytoskeleton through protein kinases ROCK and LIM-kinase. Science. 1999; 285:895–898. [PubMed: 10436159]
18. Samstag Y, John I, Wabnitz GH. Cofilin: A redox sensitive mediator of actin dynamics during T-cell activation and migration. Immunol Rev. 2013; 256:30–47. [PubMed: 24117811]
19. Radmacher M. Studying the mechanics of cellular processes by atomic force microscopy. Methods Cell Biol. 2007; 83:347–372. [PubMed: 17613316]
20. Gonnermann C, Huang C, Becker SF, Stamov DR, Wedlich D, Kashef J, Franz CM. Quantitating membrane bleb stiffness using AFM force spectroscopy and an optical sideview setup. Integr Biol. 2015; 7:356–363.
21. Zhang W, Ferguson J, Ng SM, Hui K, Goh G, Lin A, Esplugues E, Flavell RA, Abraham C, Zhao H, Cho JH. Effector CD4+ T cell expression signatures and immune-mediated disease associated genes. PLOS ONE. 2012; 7:e38510. [PubMed: 22715389]
22. Michaelson D, Silletti J, Murphy G, D'Eustachio P, Rush M, Philips MR. Differential localization of Rho GTPases in live cells: Regulation by hypervariable regions and RhoGDI binding. J Cell Biol. 2001; 152:111–126. [PubMed: 11149925]
23. Ambach A, Saunus J, Konstandin M, Wesselborg S, Meuer SC, Samstag Y. The serine phosphatases PP1 and PP2A associate with and activate the actin-binding protein cofilin in human T lymphocytes. Eur J Immunol. 2000; 30:3422–3431. [PubMed: 11093160]
24. Mempel TR, Henrickson SE, von Andrian UH. T-cell priming by dendriticcells in lymph nodes occurs in three distinct phases. Nature. 2004; 427:154–159. [PubMed: 14712275]
25. Freeman SA, Lei V, Dang-Lawson M, Mizuno K, Roskelley CD, Gold MR. Cofilin-mediated F-actin severing is regulated by the Rap GTPase and controls the cytoskeletal dynamics that drive lymphocyte spreading and BCR microcluster formation. J Immunol. 2011; 187:5887–5900. [PubMed: 22068232]
26. Samstag Y, Eckerskorn C, Wesselborg S, Henning S, Wallich R, Meuer SC. Costimulatory signals for human T-cell activation induce nuclear translocation of pp19/cofilin. Proc Natl Acad Sci USA. 1994; 91:4494–4498. [PubMed: 8183936]
27. Wabnitz GH, Nebl G, Klemke M, Schröder AJ, Samstag Y. Phosphatidylinositol 3-kinase functions as a Ras effector in the signaling cascade that regulates dephosphorylation of the actin-remodeling protein cofilin after costimulation of untransformed human T lymphocytes. J Immunol. 2006; 176:1668–1674. [PubMed: 16424196]
28. Lehmann PV, Targoni OS, Forsthuber TG. Shifting T-cell activation thresholds in autoimmunity and determinant spreading. Immunol Rev. 1998; 164:53–61. [PubMed: 9795763]
29. Tian J, Lehmann PV, Kaufman DL. Determinant spreading of T helper cell 2 (Th2) responses to pancreatic islet autoantigens. J Exp Med. 1997; 186:2039–2043. [PubMed: 9396773]
30. Faure S, Salazar-Fontana LI, Semichon M, Tybulewicz VLJ, Bismuth G, Trautmann A, Germain RN, Delon J. ERM proteins regulate cytoskeleton relaxation promoting T cell-APC conjugation. Nat Immunol. 2004; 5:272–279. [PubMed: 14758359]
31. Tybulewicz VLJ, Henderson RB. Rho family GTPases and their regulators in lymphocytes. Nat Rev Immunol. 2009; 9:630–644. [PubMed: 19696767]
32. Lu Q, Liu X, Trama J, Roti MA, Go WY, Ho SN. Identification of the cytoskeletal regulatory protein α-adducin as a target of T cell receptor signaling. Mol Immunol. 2004; 41:435–447. [PubMed: 15163540]

33. Chan KT, Creed SJ, Bear JE. Unraveling the enigma: Progress towards understanding the coronin family of actin regulators. Trends Cell Biol. 2011; 21:481–488. [PubMed: 21632254]

34. Morley SC, Sung J, Sun G-P, Martelli MP, Bunnell SC, Bierer BE. Gelsolin overexpression alters actin dynamics and tyrosine phosphorylation of lipid raft-associated proteins in Jurkat T cells. Mol Immunol. 2007; 44:2469–2480. [PubMed: 17178161]

35. Freeman SA, Jaumouillé V, Choi K, Hsu BE, Wong HS, Abraham L, Graves ML, Coombs D, Roskelley CD, Das R, Grinstein S, Gold MR. Toll-like receptor ligands sensitize B-cell receptor signalling by reducing actin-dependent spatial confinement of the receptor. Nat Commun. 2015; 6:6168. [PubMed: 25644899]

36. Davies SP, Reddy H, Caivano M, Cohen P. Specificity and mechanism of action of some commonly used protein kinase inhibitors. Biochem J. 2000; 351:95–105. [PubMed: 10998351]

37. Ishizaki T, Naito M, Fujisawa K, Maekawa M, Watanabe N, Saito Y, Narumiya S. p160^{ROCK}, a Rho-associated coiled-coil forming protein kinase, works downstream of Rho and induces focal adhesions. FEBS Lett. 1997; 404:118–124. [PubMed: 9119047]

38. Xiao N, Eto D, Elly C, Peng G, Crotty S, Liu Y-C. The E3 ubiquitin ligase Itch is required for the differentiation of follicular helper T cells. Nat Immunol. 2014; 15:657–666. [PubMed: 24859451]

39. Bruce MA, Butte MJ. Real-time GPU-based 3D deconvolution. Opt Express. 2013; 21:4776–4773.

40. Rico F, Roca-Cusachs P, Gavara N, Farré R, Rotger M, Navajas D. Probing mechanical properties of living cells by atomic force microscopy with blunted pyramidal cantilever tips. Phys Rev E Stat Nonlin Soft Matter Phys. 2005; 72:021914. [PubMed: 16196611]

41. Agarwal, S., Mierle, K., et al. Ceres Solver. http://ceres-solver.org

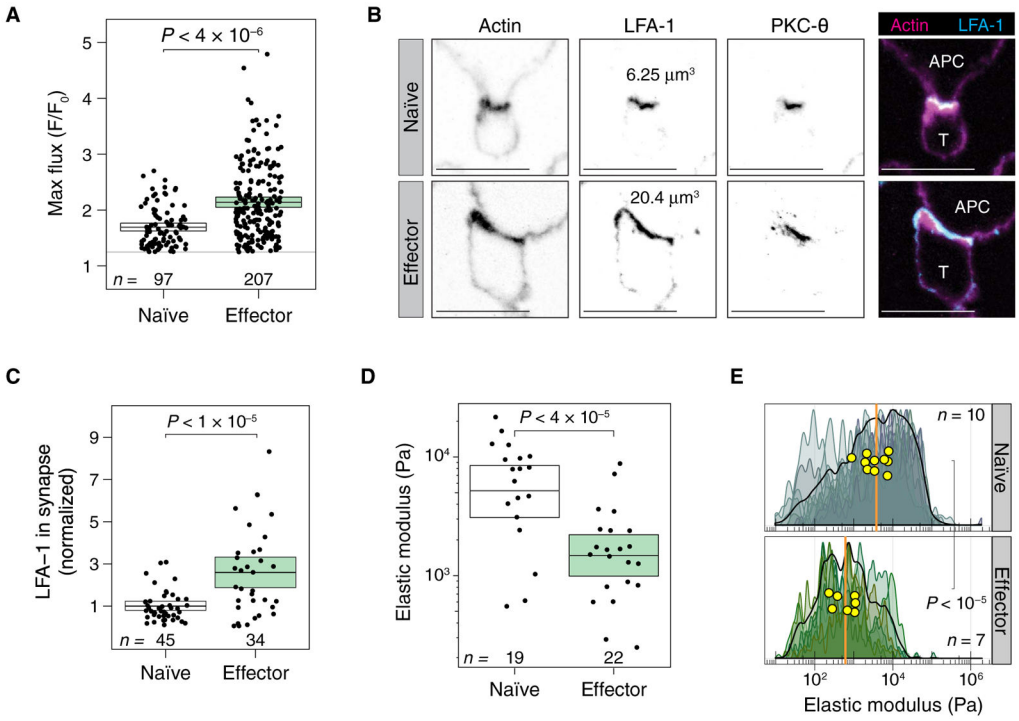

Fig. 1. Compared to naïve CD4$^+$ T cells, effector CD4$^+$ T cells are more reactive, form larger immune synapses, and are mechanically softer

(**A**) Maximum Ca^{2+} flux responses in naïve and effector OT-II T cells interacting with antigen-pulsed APCs. Each dot represents an individual T cell. Maximum fluorescence was calculated as an average over the whole cell. Ca^{2+} flux was scaled to the brightness of each cell at time 0. Boxes show means and 95% confidence interval (CI) values. The numbers of Ca^{2+} fluxes measured for each group in a single experiment are shown. Results are representative of two independent experiments. (**B**) Immune synapses formed by naïve (top) and effector (bottom) OT-II T cells interacting with antigen-pulsed APCs were imaged by confocal microscopy. Images show a single confocal slice through the middle of the immune synapse. Representative cells that had the median volume of LFA-1$^+$ voxels were chosen. Images are representative of 151 total cells from two independent experiments. (**C**) Effector T cells have a larger volume of LFA-1$^+$ voxels in the immune synapse. The total volume of LFA-1 represents the size of the immune synapse. The average immune synapse size for naïve cells was normalized to 1. Each dot represents an immune synapse between a T cell and an APC. Boxes show means and 95% CI values. The numbers of synapses measured for each group in a single experiment are shown. Results are representative of two independent experiments. (**D**) Elastic moduli derived from nanoindentation measurements for live naïve and effector T cells. Each dot is the average of about five measurements of single T cells. Boxes show means and 95% CI values. The numbers of cells measured for each group in a single experiment are shown. Results are representative of two independent experiments. (**E**) Stiffness mapping of naïve (top) and effector (bottom) T cells. Smoothed density histograms comprising ~160 nanoindentation measurements for each cell are shown. Each shade represents a distinct cell that was measured. The stiffness maps of individual T cells showed a range of elastic moduli from ~100 Pa to 100 kPa, with median stiffness for each cell shown

in yellow circles. The median stiffness values for the touches on naïve or effector cells are shown as orange vertical lines. The numbers of cells measured for each group in a single experiment are shown. Results are representative of three independent experiments.

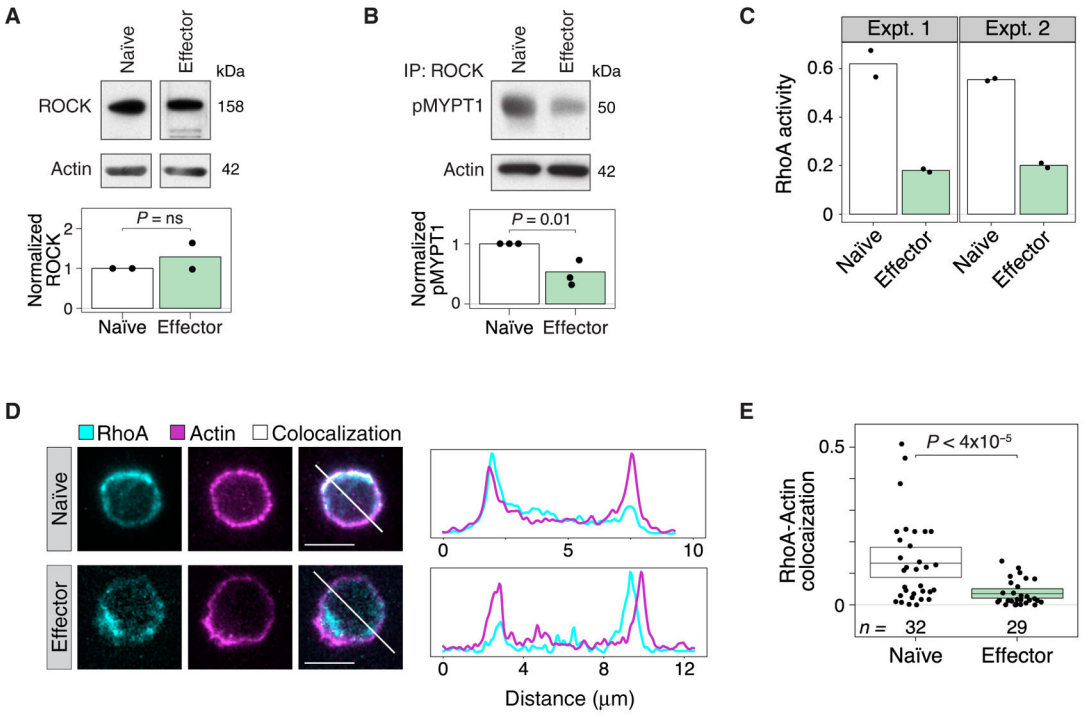

Fig. 2. RhoA and ROCK are more active in naïve CD4$^+$ T cells than in effector CD4$^+$ T cells

(**A**) Naïve and effector CD4$^+$ T cells were analyzed by Western blotting to determine the relative amounts of ROCK protein normalized to that of β-actin. The bar graph shows a densitometric analysis of relative band intensities (normalized to actin). Western blots are representative of two independent experiments. (**B**) ROCK activity in naïve and effector CD4$^+$ T cells was determined by immunoprecipitation (IP) of ROCK and incubating the immunoprecipitated samples with purified MYPT1, a ROCK substrate. The relative abundance of phospho-MYPT1 normalized to the amount of actin in the cell lysates was determined by Western blotting analysis. The bar graph shows a densitometric analysis of relative band intensities. Western blots are representative of three independent experiments. (**C**) RhoA activity in naïve and effector T cell lysates was assessed by determining the amounts of GTP-bound RhoA in each sample. Total protein in the lysates was normalized before the assay was performed. Results from two independent experiments are shown. Dots represent technical replicates for each sample. (**D** and **E**) Single slices of fluorescence three-dimensional confocal microscopy images of naïve (top) and effector (bottom) T cells stained with anti-RhoA antibody and phalloidin (D). White regions indicate colocalization of RhoA and actin. The representative cells chosen lie within 30% of the mean colocalization in (E). White diagonal lines are shown as a line profile to the right of each figure. (E) Manders coefficient values of the fluorescence colocalization of RhoA with F-actin in naïve and effector T cells. Each dot represents an individual T cell. Boxes show the means and 95% CI values. Results are representative of two independent experiments.

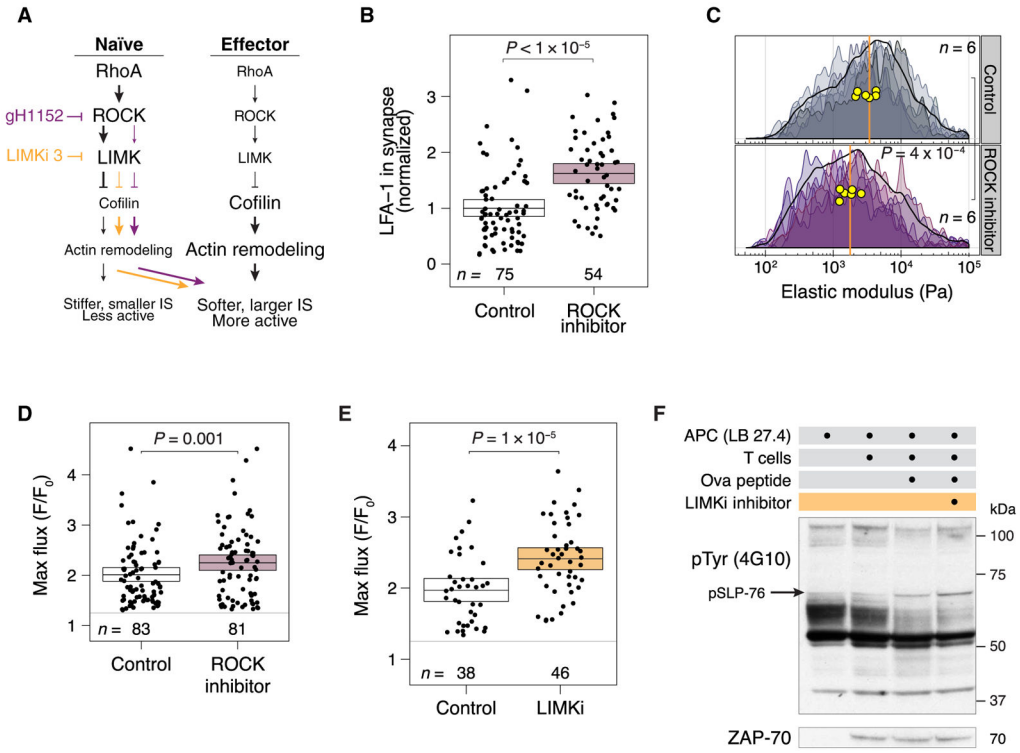

Fig. 3. Inhibition of ROCK or LIMK in naïve CD4$^+$ T cells increases the sizes of the immune synapses that they form and enhances their responses to antigen

(**A**) Pharmacological inhibition of ROCK or LIMK is hypothesized to soften T cells, enhance immune synapse size, and increase signaling. (**B**) Volume of LFA-1$^+$ voxels in the immune synapses of naïve OT-II CD4$^+$ T cells pretreated for 1 hour with the ROCK inhibitor glycyl-H-1152 or vehicle and then cocultured with antigen-pulsed APCs for 5 min. The average sizes of the immune synapses in control cells were normalized to 1. Each dot represents an immune synapse from a single T cell–APC conjugate. Boxes show means and 95% CI values. Results are representative of three independent experiments. (**C**) Stiffness mapping of naïve T cells treated for 1 hour with the ROCK inhibitor or vehicle, which is shown as a density histogram as described in Fig. 1E. Results are representative of two independent experiments. (**D** and **E**) Maximum Ca^{2+} flux responses in naïve OT-II T cells treated for 1 hour with (D) a ROCK inhibitor or (E) a LIMK inhibitor or vehicle control in the presence of antigen-pulsed APCs. Each dot represents an individual T cell. Maximum fluorescence was calculated by Imaris as an average over each cell. Ca^{2+} flux was scaled to the brightness of each cell at time 0. Boxes show means and 95% CI values. Results are representative of three (ROCK inhibitor) or two (LIMK inhibitor) independent experiments. (**F**) Naïve OT-II T cells were pretreated with a LIMK inhibitor or vehicle and then incubated for 5 min with antigen-pulsed APCs. The cells were analyzed by Western blotting with antibodies against the indicated targets. Western blots are representative of two independent experiments.

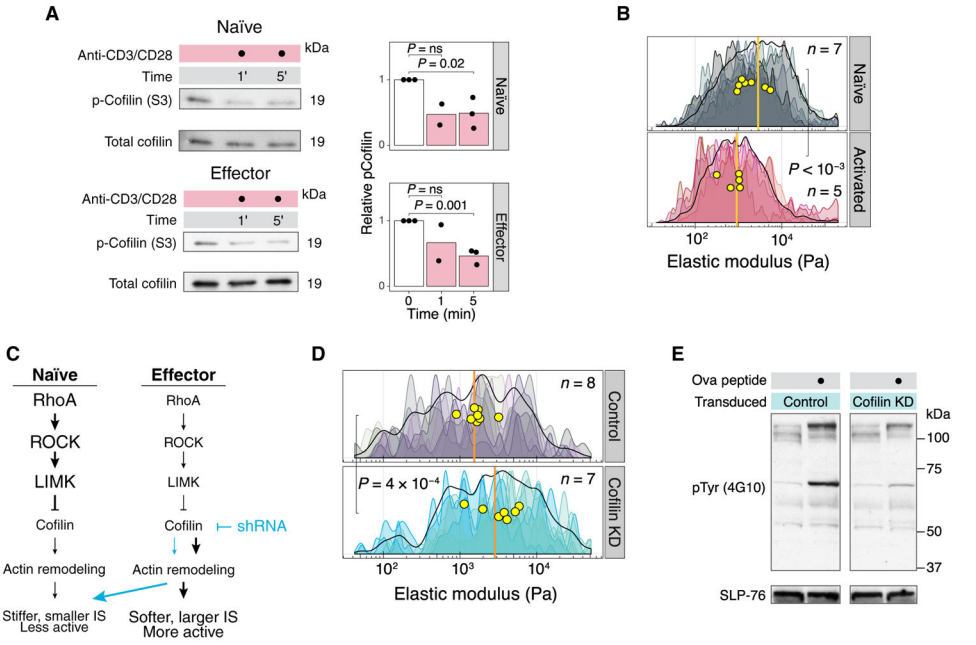

Fig. 4. Cofilin controls the stiffness and activation of T cells

(**A**) Naïve and effector T cells were stimulated with plate-bound anti-CD3 and anti-CD28 antibodies for the indicated times. The cells were lysed directly in SDS loading buffer and analyzed by Western blotting with antibodies against the indicated proteins. The amounts of phosphorylated cofilin were normalized to those of total cofilin. The bar graphs show densitometric analyses of relative band intensities. Western blots are representative of three independent experiments. (**B**) AFM stiffness mapping of naïve T cells after 1-hour incubation on coverslips coated with poly-D-lysine (Naïve) or poly-D-lysine and anti-CD3ε (Activated). Results are representative of two independent experiments. (**C**) Knocking down cofilin in effector T cells is hypothesized to increase cell stiffness and decrease both immune synapse size and the extent of activation. (**D**) Stiffness mapping of effector T cells expressing cofilin-specific shRNA or control shRNA, which is shown as a density histogram as described in Fig. 1E. Results are representative of two independent experiments. (**E**) Effector OT-II T cells expressing control shRNA or cofilin-specific shRNA were incubated for 5 min with antigen-pulsed APCs. The cells were then analyzed by Western blotting with an antibody against phosphotyrosine. Blots were probed with SLP-76 as a loading control. Western blots are representative of two independent experiments.

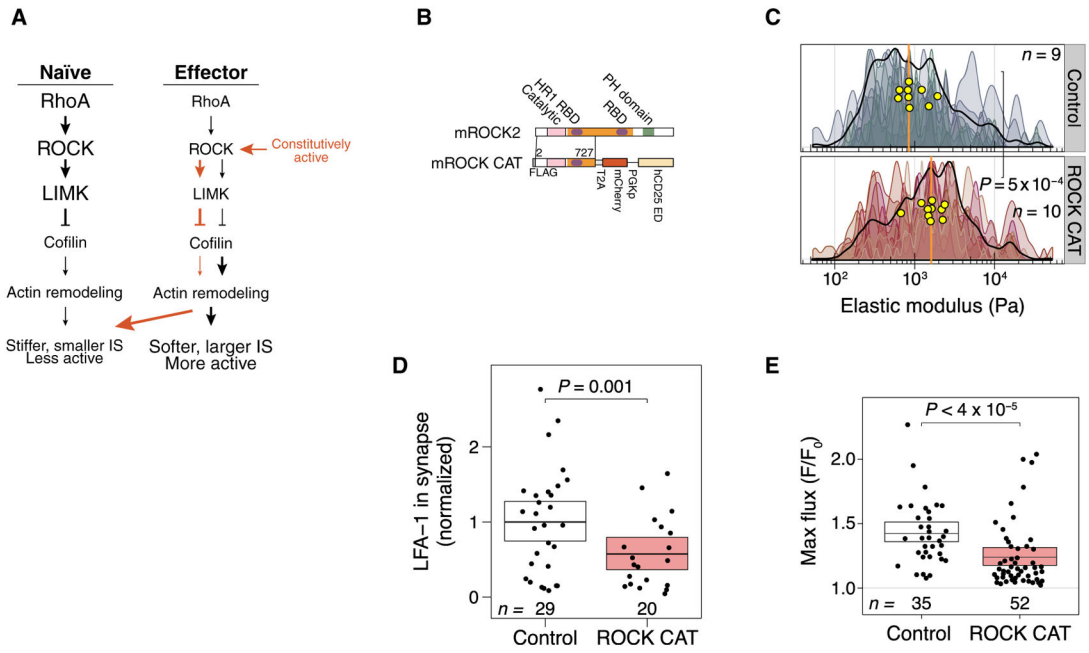

Fig. 5. Expression of constitutively active ROCK in effector CD4$^+$ T cells reduces immune synapse size and T cell responses

(**A**) Increased ROCK activity in effector CD4$^+$ T cells is hypothesized to increase cellular stiffness and decrease both immune synapse size and the extent of activation. (**B**) Domain structure in full-length ROCK2 and a truncated ROCK that is catalytically active ("ROCK CAT") because of the deletion of a regulatory Rho-binding domain. FLAG, the polypeptide DYKDDDDK tag; RBD, Rho-binding domain; T2A, self-cleaving 2A peptide; PH, pleckstrin homology domain; PGKp, phosphoglycerol kinase promoter. (**C**) Stiffness mapping of effector T cells transduced with control virus or with virus expressing the ROCK CAT mutant. Data are shown as a density histogram described in Fig. 1E. (**D**) Volumes of LFA-1$^+$ voxels in the immune synapses formed by effector OT-II T cells transduced with control virus or virus expressing the ROCK CAT mutant. The average sizes of the immune synapses in the control cells were normalized to 1. Each dot represents the immune synapse from a single T cell–APC conjugate. Boxes show means and 95% CI values. Results are representative of two independent experiments. (**E**) Maximum Ca^{2+} flux responses in effector OT-II T cells transduced with control virus or virus expressing the ROCK CAT mutant after making contact with coverslips coated with anti-CD3ε antibody. Data are shown as described in Fig. 1E. Boxes show means and 95% CI values. Results are representative of two independent experiments.